Buckling of a stiff film bound to a compliant substrate (part I). Formulation, linear stability of cylindrical patterns, secondary bifurcations

Basile Audoly

Institut Jean le Rond d'Alembert, UMR 7190 du CNRS, CNRS/Université Pierre et Marie Curie, 4 place Jussieu, F-75252 Paris Cedex 05

Arezki Boudaoud

Laboratoire de Physique Statistique, UMR 8550 du CNRS/Paris 6/Paris 7 École normale supérieure, 24 rue Lhomond, F-75231 Paris Cedex 05

Abstract

The buckling of a thin elastic film bound to a compliant substrate is studied: we analyze the different patterns that arise as a function of the biaxial residual compressive stress in the film. We first clarify the boundary conditions to be used at the interface between film and substrate. We carry out the linear stability analysis of the classical pattern made of straight stripes, and point out secondary instabilities leading to the formation of undulating stripes, varicose, checkerboard or hexagonal patterns. Straight stripes are found to be stable only in a narrow window of load parameters. We present a weakly nonlinear post-buckling analysis of these patterns: for equi-biaxial residual compression, straight wrinkles are never stable and square checkerboard patterns are found to be optimal just above threshold; for anisotropic residual compression, straight wrinkles are present above a primary threshold and soon become unstable with respect to undulating stripes. These results account for many of the previously published experimental or numerical results on this geometry.

Key words: Buckling, Plates, Thermal stress, Asymptotic analysis, Energy methods

1 Introduction

The buckling of multi-layered materials is a classical subject in mechanics and has received continuous attention due to its importance in the design of sandwich panels (Allen, 1969). Recent efforts in this field were motivated by the understanding of wrinkles generation in human skin, or by applications to the templating and assembly of materials (see e.g. Genzer and Groenewold, 2006, for a review).

In this paper, we consider the buckling of a thin and stiff film bonded to a compliant substrate. This can be realized experimentally by depositing a thin metallic film onto an elastomer (Bowden et al., 1998; Huck et al., 2000; Yoo et al., 2002) and letting the system cool down at room temperature. Due to the mismatch in thermal expansion coefficients between the film and substrate, residual stress is induced in the film. Another experimental realization uses gels (Sultan and Boudaoud, 2007), for which swelling by absorption of a liquid replaces thermal expansion. When the residual stress is compressive, it can lead to buckling into straight wrinkles (Bowden et al., 1998), a pattern that has cylindrical symmetry, *i. e.* is invariant in one direction. Secondary patterns may also appear; the crests and valleys of the wrinkles can organize into labyrinthine patterns (Bowden et al., 1998) or zigzag patterns, also named herringbone or chevron (Huck et al., 2000); yet another pattern, called square checkerboard, can be formed when maxima and minima of the film deflection are distributed at the vertices of a square lattice (Yoo et al., 2002).

These patterns have been investigated numerically. Chen and Hutchinson (2004) studied periodic checkerboard or herringbone patterns by simulating a single elementary cell, a square or a parallelogram. Huang et al. (2004) first considered the case of a Winkler foundation, and later (Huang et al., 2005) the case of a thick elastic foundation; they observed straight wrinkles, checkerboard, labyrinths or herringbone patterns depending on the loading conditions.

The stability analysis of the unbuckled state, which yields the critical differential strain and the wavelength of the wrinkles at threshold, is now classical (Allen, 1969). In order to determine the amplitude of the wrinkles, Chen and Hutchinson (2004) performed a nonlinear analysis of the cylindrical patterns, which was later extended to the case of a substrate with finite depth by Huang et al. (2005). Independently, Mahadevan and Rica (2005) proposed an analysis of herringbone patterns based on amplitude equations; this approach is suited to the analysis of large wavelength perturbations on top of the straight wrinkles, an assumption that does not apply to the geometry of herringbones.

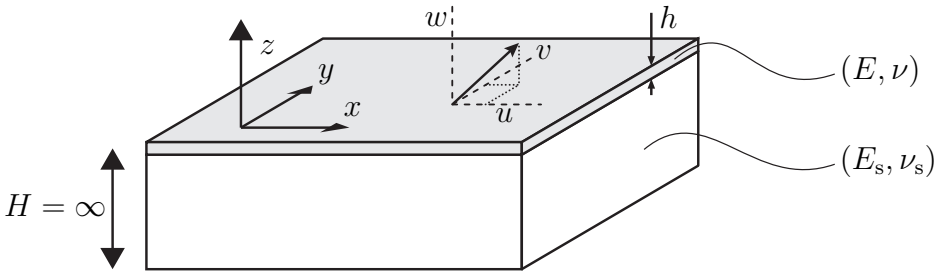

Fig. 1. Geometry of the problem and notations.

The stability of cylindrical patterns has not been addressed analytically. Can one explain the variety of patterns reported in the literature using the classical model of a plate with residual compressive stress on an elastic foundation? Under what loading can each type of pattern be observed? What are their amplitudes and wavelengths? These questions will be addressed here. The present contributions are twofold: we first clarify the boundary conditions to be used at the interface between film and substrate; in a second step, we analyze the linear stability of the cylindrical pattern and show that it can become unstable with respect to undulating stripes, varicose, checkerboard, and hexagonal patterns.

The paper is organized as follows. Section 2 recalls the classical formulation of the problem and the expression of the elastic energy of the system. In Section 3, we determine the boundary conditions at the interface between the film and the substrate and derive the effective stiffness of the foundation. The linear stability of the straight wrinkles is studied in section 4. The following two sections deal with the nonlinear analysis of the secondary patterns: undulating stripes in Section 5, checkerboards and hexagons in Section 6. We conclude in Section 7 by summarizing our results and showing their relevance to previous experimental and numerical studies.

2 Formulation

We consider a thin elastic film bound to an elastic foundation, which buckles under residual biaxial compressive stress. In the following, we write the elastic energy of the system, remaining in the framework Hookean elasticity (linear elastic response). The film is described by the Föppl–von Kármán theory (FvK) for thin elastic plates (Timoshenko and Gere, 1961) undergoing moderate (but nonzero) deflections, while the foundation is considered to be a half-infinite linearly elastic solid.

2.1 Film

We denote E, ν and h the Young's modulus, Poisson's ratio and thickness of the film, respectively, see Fig. 1. The reduced Young's modulus, E^*, is defined as

$$E^* = \frac{E}{1-\nu^2}. \tag{1}$$

In order to define the residual stress in the film, assumed to be homogeneous, we consider the configuration such that the substrate is in its natural configuration (this is not necessarily a stable equilibrium). Let $(-\eta_x)$ and $(-\eta_y)$ denote the principal strains in the film in this configuration, with respect to the natural configuration of the film; let the in-plane x and y axes be aligned with the associated principal strain directions; then, z is the direction perpendicular to the mean plane of the film (see Fig. 1 for the geometry and notations). The differential strain (η_x, η_y) is the load parameter of the system.

In the deformed configuration, the displacement of the center-surface of the film is noted $(u(x,y), v(x,y), w(x,y))$, where (u, v) are the in-plane components and w the deflection. The strain in deformed configuration is calculated using a classical approximation, first introduced by Föppl, that consists in neglecting all nonlinear terms depending on the in-plane displacement u or v. The strain tensor is then defined as

$$\epsilon_{xx} = -\eta_x + \frac{\partial u}{\partial x} + \frac{1}{2}\left(\frac{\partial w}{\partial x}\right)^2, \tag{2a}$$

$$\epsilon_{xy} = \frac{1}{2}\left(\frac{\partial u}{\partial y} + \frac{\partial v}{\partial x} + \frac{\partial w}{\partial x}\,\frac{\partial w}{\partial y}\right), \tag{2b}$$

$$\epsilon_{yy} = -\eta_y + \frac{\partial v}{\partial y} + \frac{1}{2}\left(\frac{\partial w}{\partial y}\right)^2. \tag{2c}$$

The stress tensor is given by Hookean elasticity (plane stress) as

$$\sigma_{xx} = \frac{E}{1-\nu^2}(\epsilon_{xx} + \nu\,\epsilon_{yy}), \tag{3a}$$

$$\sigma_{xy} = \frac{E}{1+\nu}\epsilon_{xy}, \tag{3b}$$

$$\sigma_{yy} = \frac{E}{1-\nu^2}(\epsilon_{yy} + \nu\,\epsilon_{xx}). \tag{3c}$$

The load parameter (η_x, η_y) can be related to the biaxial residual compressive stress $(\sigma^0_{xx}, \sigma^0_{yy})$ in the film by the constitutive equations above

$$\sigma^0_{xx} = -E^*\,(\eta_x + \nu\,\eta_y), \qquad \sigma^0_{xy} = 0, \qquad \sigma^0_{yy} = -E^*\,(\nu\,\eta_x + \eta_y).$$

In plate theory, the energy $\mathcal{E}_\mathrm{f}$ of the film per unit area is the sum of a stretching contribution $\mathcal{E}_\mathrm{fs}$ and a bending contribution $\mathcal{E}_\mathrm{fb}$:

$$\mathcal{E}_\mathrm{f} = \mathcal{E}_\mathrm{fs} + \mathcal{E}_\mathrm{fb}, \tag{4}$$

which take the following form

$$\mathcal{E}_\mathrm{fs} = \frac{1}{L_x\,L_y}\,\frac{h}{2}\int \sigma_{\alpha\beta}\,\epsilon_{\alpha\beta}\,\mathrm{d}x\,\mathrm{d}y, \tag{5}$$

$$\mathcal{E}_\mathrm{fb} = \frac{1}{L_x\,L_y}\,\frac{D}{2}\int (\Delta w)^2\,\mathrm{d}x\,\mathrm{d}y, \tag{6}$$

where L_x and L_y define the size of the rectangular domain considered, which is assumed to be very large compared to all other dimensions — we are actually considering an infinite domain but formally introduce two large lengths L_x and L_y which allow us to write easily averages per unit area, such as the ones written above for the energy. By convention, Greek indices run over in-plane directions: above, α and β can take the values x or y. The bending modulus of the film is defined, for a homogeneous and isotropic material, as

$$D = \frac{E\,h^3}{12\,(1-\nu^2)}. \tag{7}$$

2.2 Substrate

The substrate, which fills the half-space $z < -h/2$, has a Young's modulus E_s and Poisson's ratio ν_s. Introducing the Fourier transform of the film deflection

$$\hat{w}(k_x,k_y) = \int \mathrm{d}x\ \mathrm{d}y\ w(x,y)\exp[-i(k_x x + k_y y)], \tag{8}$$

where $i=\sqrt{-1}$, the energy of substrate, which is described by linear elasticity, can be written as the sum of the energies of each Fourier mode:

$$\mathcal{E}_\mathrm{s} = \frac{1}{L_x\,L_y}\int \mathrm{d}k_x\ \mathrm{d}k_y\,E_\mathrm{s}^*\sqrt{k_x^2+k_y^2}\,\hat{w}(k_x,k_y)\,\hat{w}(-k_x,-k_y). \tag{9}$$

Its dependence on the substrate's material properties is collected into a single parameter, E_s^*, which is proportional to E_s and is a function of Poisson's ratio ν_s. This dependence on ν_s reflects the relevant choice of boundary conditions to be imposed the interface between the film and the substrate, which we shall elucidate in Section 3; until then, we leave this dependence undetermined, through a function $e(\nu_\mathrm{s})$, given later in equation (15):

$$E_\mathrm{s}^* = E_\mathrm{s}\,e(\nu_\mathrm{s}). \tag{10}$$

Note that the star notation for E_{s}^* does not imply that its dependence takes the same form as in equation (1) for the film.

2.3 Optimization problem

The equilibrium states of the system are those that minimize the total energy:

$$\mathcal{E}_{\mathrm{t}}(\{u,v,w\}) = \mathcal{E}_{\mathrm{s}}(\{w\}) + \mathcal{E}_{\mathrm{fb}}(\{w\}) + \mathcal{E}_{\mathrm{fs}}(\{u,v,w\}). \tag{11}$$

We employ curly braces to stress on the fact that these energies are functionals of u, v and w, *i. e.* that they depend on all the values of the functions $u(x,y)$, $v(x,y)$ and $w(x,y)$. This energy has to be minimized with respect to the displacement $(u(x,y), v(x,y), w(x,y))$, for given values of the material parameters and differential strain (η_x, η_y). The main purpose of this paper is to find minimizers of this energy for various values of the parameters.

2.4 Classical buckling analysis: cylindrical patterns

The planar configuration $u = v = w = 0$ is always a solution to the equations of equilibrium corresponding to the energy (11). Its linear stability is a classical topic Allen (1969): this planar configuration is stable below a critical compressive strain and buckles above it. The buckling mode has the form

$$w(x,y) = A\,\cos(k\,x).$$

We refer to this pattern as the *cylindrical pattern*. Here and everywhere in the paper, 'cylinder' has to be understood in its mathematical meaning of a geometric surface invariant by translation along a direction, which does not necessarily have a circular cross-section — here, the 'cross-section' is a sinusoid.

In the case of isotropic [1] compression $\eta_x = \eta_y = \eta$, the buckling threshold and wavenumber are

$$\eta_{\mathrm{c}}^I = \frac{1}{1+\nu}\left(\frac{3\,E_{\mathrm{s}}^*}{2\,E^*}\right)^{2/3} \tag{12a}$$

and

$$k = \frac{1}{h}\left(\frac{12\,E_{\mathrm{s}}^*}{E^*}\right)^{1/3}. \tag{12b}$$

It turns out that this sinusoidal buckling mode is an exact solution of the nonlinear equations for a plate on an elastic foundation, even at finite distance

[1] Here we use 'isotropic' as a synonym for 'equi-biaxial'. There is no ambiguity as we do not need to consider the transverse direction for the film.

above the buckling threshold. Based on this remark, Chen and Hutchinson (2004) found the amplitude of the post-buckled pattern:

$$A = h \left(\frac{\eta}{\eta_{\mathrm{c}}^I} - 1 \right)^{1/2} . \tag{12c}$$

Remarkably enough, the wavelength that is unstable at threshold is the one with lowest energy above threshold: k depends on the material parameters but not on the load parameters η_x or η_y.

3 Effective stiffness of the substrate

In this section, we return to the formulation of the problem and compute the effective modulus E_{s}^* associated with the deformations of the substrate. To this end, we derive the boundary conditions to be enforced at the interface between film and substrate. It is not clear what boundary conditions should be written there [2]. On one hand, the Föppl–von Kármán (FvK) energy of the film is derived under the assumption that no traction is applied along the lower and upper edges of the plate, and so this implies that no force is transmitted along the interface. On the other hand, the film is bound to the substrate, and the displacement must be continuous at the interface. One cannot impose both free boundary conditions and imposed displacement at the interface as this would involve too many boundary conditions for the film. This point seems to be unsettled so far; without a rigorous justification, Huang et al. (2005) choose to impose vanishing longitudinal tractions on top of substrate while Huang (2005) imposes a vanishing longitudinal displacement on top of substrate. Chen and Hutchinson (2004) discusses both types of boundary conditions.

The key remark is that the plate equations can be derived from 3D elasticity by expansion with respect to a small parameter. In this expansion, the in-plane and the transverse stress come with different orders of magnitudes: the transverse stress is much smaller. In contrast, both the in-plane and the transverse stress components are *a priori* of comparable magnitude in the substrate as it is described by a theory with no small or large parameter. As we shall show, the normal stress σ_{zz} imposed by the substrate at the interface is relevant for

[2] Determining which boundary conditions must be enforced in an asymptotic (plate, rod or shell) problem is a tricky question. For instance, it is well known that it is not consistent to enforce boundary conditions imposing different displacements on both sides of a plate, eventhough this is possible for a thick elastic medium. Here, the problem is similar: we show that it is not consistent to enforce the continuity of tangential tractions at the interface when the film is very thin.

the equilibrium of the film and is balanced by bending terms. In contrast, the shear stress $\sigma_{z\alpha}$ (with $\alpha = x, y$) imposed by the substrate at the interface is negligible in front the large tensile stress from the film's perspective.

To determine the boundary conditions at the interface, one can in principle proceed as follows. The displacement $(u(x, y), v(x, y), w(x, y))$ at the interface is first set arbitrarily; the equations of equilibrium are then solved in the substrate and, in particular, the traction applied at the interface by the substrate onto the film is derived; the equations for the film are solved with these imposed traction at the edges; this leads ultimately to the deformed shape of the film. The actual solution is found by requiring that this deformed shape of the film is consistent with the displacement $(u(x, y), v(x, y), w(x, y))$ that was assumed at the beginning of the procedure. This warrants the continuity of displacement at the interface. In what follows, we outline the implementation of this approach and derive the effective boundary conditions to be applied at the interface.

We shall first make three assumptions, which are relevant to the limits we consider, namely that strain is small, that the film's slope is everywhere small, and that the substrate is very compliant with respect to the film *i. e.* the contrast of elastic moduli is large, $C = E^*/E^*_{\mathrm{s}} \to \infty$:

(1) the in-plane displacement (u, v) is of order w^2/λ;
(2) $w/\lambda \ll 1$;
(3) $C\,(w\,h)/\lambda^2 \gg 1$.

These assumptions will be checked to be consistent at the end. Here, $\lambda \sim 2\pi/k$ is the typical wavelength of the pattern. The first two conditions are scaling assumptions underlying the Föppl-von Kármán (FvK) plate theory. These two conditions imply in particular that the in-plane displacement u and v are much smaller than the transverse one, w. Note that these assumptions are consistent with the weakly post-buckled cylindrical buckling, as described by equations (12): for this particular pattern, the conditions 1 and 2 follow directly from the scalings of the FvK equations; for condition 3, we get $C(wh)/\lambda^2 \sim C(Ah)k^2 \sim C\,C^{-2/3} = C^{1/3}$ which is indeed a large number by assumption.

By assumptions 1 and 2, u and v are much smaller than w. As a result, and from the substrate's perspective, the boundary conditions to be applied at the interface should be the continuity of the deflection w, and also $u = v = 0$ (plane strain). The elasticity of a half-infinite domain with purely transverse displacement applied at its boundary is solved by elementary methods Allen

(1969). The resulting stress at the interface is given by its Fourier components

$$\begin{pmatrix} \hat{\sigma}^{\rm int}_{xz}(k_x,k_y) \\ \hat{\sigma}^{\rm int}_{yz}(k_x,k_y) \\ \hat{\sigma}^{\rm int}_{zz}(k_x,k_y) \end{pmatrix} = \frac{E_{\rm s}}{(1+\nu_{\rm s})(3-4\nu_{\rm s})} \begin{pmatrix} i\,(1-2\nu_{\rm s})\,k_x \\ i\,(1-2\nu_{\rm s})\,k_y \\ 2\,(1-\nu_{\rm s})\,\sqrt{{k_x}^2+{k_y}^2} \end{pmatrix} \hat{w}(k_x,k_y). \quad (13)$$

As outlined earlier, we shall now solve the plate problem, and determine the shape of the film subjected to a force per unit area $f = (f_x, f_y, f_y)$ along its lower interface, with $f_i = -\sigma^{\rm int}_{iz}$, where $\sigma^{\rm int}_{iz}$ is the inverse Fourier transform of the left-hand side of equation (13).

For this plate problem, first consider the case of purely normal applied forces, that is set the tangential traction $f_x = -\sigma^{\rm int}_{xz}$ and $f_y = -\sigma^{\rm int}_{yz}$ to zero. Then, the constitutive equations (3) in the film yield $\sigma_{\alpha\beta} = \mathcal{O}(E\,\epsilon_{\alpha\beta})$, where the $\mathcal{O}$ notation means 'is of the same order of magnitude or smaller'. By the definition of strain, $\epsilon_{\alpha\beta} = \mathcal{O}((w/\lambda)^2)$. Therefore, $\sigma_{\alpha\beta} = \mathcal{O}(E\,(w/\lambda)^2) = \mathcal{O}(E\,k^2\,w^2)$, where $k = 2\pi/\lambda$ is the typical wavenumber of the patterns.

When the in-plane interface traction f_x and f_y at the interface are properly considered, the solution outlined at the previous paragraph must be corrected with a new, inhomogeneous term in the equation for the in-plane equilibrium of the film:

$$h\,\frac{\partial \sigma_{\alpha\beta}}{\partial x_\beta} = f_\alpha,$$

where Greek indices like α again range over in-plane directions, x and y. However, it turns out that this correction is very small in the limit we consider. Indeed, consider the ratio ρ of the source term f_α in the previous equation, to the typical value of the left-hand side as determined in the previous paragraph with $f_\alpha = 0$. This ratio reads

$$\rho = \frac{f_\alpha}{h\,\frac{\partial \sigma_{\alpha\beta}}{\partial x_\beta}}$$

The numerator $f_\alpha = -\sigma^{\rm int}_{\alpha z}$ can be estimated as $f_\alpha \sim E_{\rm s}\,k\,w$ from equation (13). The denominator can be estimated as $h\,k\,\sigma_{\alpha\beta}$, using the estimate given previously for the in-plane stress $\sigma_{\alpha\beta}$. Combining all this yields:

$$\rho \sim \frac{E_{\rm s}\,k\,w}{E\,h\,k^3\,w^2} \sim \frac{1}{C\,h\,k^2\,w} \quad (14)$$

By our assumption (3), this is the inverse of a large number, and $\rho \ll 1$: the tangential traction applied by the substrate at the interface does not significantly affect the solution for the film. By neglecting the tangential forces applied on the film, one makes a negligible error [3]. This justifies the use of

[3] The subtle point is that, although the transverse force f_z is of the same order

the energy (4) for the film, which implicitly assumes that no in-plane traction is applied [4]. This argument shows as well that there is no point to enforce the continuity of the tangential stress at the interface, the stress applied by the substrate being negligible from the film's perspective anyway.

Therefore, the boundary conditions to be used for the substrate at the interface are $u = 0$, $v = 0$, and the continuity of σ_{zz}. In this framework, the Fourier components of the interfacial deflection $\hat{w}$ are related to the interface normal stress by:

$$\hat{\sigma}_{zz}^{\mathrm{int}}(k_x, k_y) = 2E_{\mathrm{s}}^{*}\, \hat{w}(k_x, k_y)\, \sqrt{{k_x}^2 + {k_y}^2},$$

where the effective stiffness E_{s}^{*} is found by identification with equation (13):

$$E_{\mathrm{s}}^{*} = E_{\mathrm{s}}\, e(\nu_{\mathrm{s}}), \quad \text{where } e(\nu_{\mathrm{s}}) = \frac{1-\nu_{\mathrm{s}}}{(1+\nu_{\mathrm{s}})(3-4\nu_{\mathrm{s}})}. \tag{15}$$

After integration over the variables x, y and z, one obtains the elastic energy of the substrate per unit area in the form of equation (9).

It is erroneous to replace the boundary condition $u = v = 0$ at the interface by $\sigma_{\alpha z} = 0$. With these boundary conditions, the in-plane displacements u and v can be calculated and they are of the same order of magnitude as w at equilibrium. By continuity of the displacements at the interface, this leads to an in-plane strain in the film of order $\epsilon_{\alpha\beta} \sim w/\lambda$. The stretching energy in the film is then of order $Eh(w/\lambda)^2$, to be compared to its bending energy, of order $Eh^3(w/\lambda^2)^2$. This would imply that the stretching energy in the film is much larger than its bending energy — roughly $(\lambda/h)^2$ times larger to be accurate. In these conditions, it is inconsistent to use the FvK theory.

4 Linear stability of the cylindrical pattern

Having clarified the formulation of the problem, we proceed to the analysis of buckling of a thin film bound to a compliant substrate. We take advantage of the existence of an exact solution to the post-buckling problem, describing the cylindrical pattern, to carry out the stability analysis. This calculation has some similarities with the analysis of stability of the Euler rod solution in a long rectangular plate clamped along its long edges and subjected to biaxial

---

of magnitude as the in-plane ones, f_α, by equation (13), f_z cannot be neglected as the film is much more compliant to imposed transverse displacements to which it reacts by bending, than to imposed in-plane displacements to which is reacts by stretching.

[4] If longitudinal force applied on the film at the interface were not negligible, one would have to include in the energy of the film an additional potential term, proportional to the in-plane displacements u and v.

stress (Jensen, 1993; Audoly, 1999; Audoly et al., 2002; Audoly and Pomeau, 2008).

4.1 Perturbed deflection $w(x, y)$

As noted in Section 2.4, an exact solution $w(x, y) = A\cos(k\,x)$ describing the post-buckled cylindrical pattern is available (Chen and Hutchinson, 2004). We call this solution the cylindrical base state. In the present Section, we analyze its stability when subjected to infinitesimal perturbations. We show that this well-studied pattern is in fact stable in a very limited window of load parameters.

To this end, we introduce a perturbation to the deflection in the form $w(x, y) = A\cos(k\,x) + \delta w(x, y)$. In bifurcation analysis, the symmetries of the base solution can be exploited (Manneville, 1990). Indeed, according to a general result, it is sufficient to consider perturbations (linearly unstable modes) that are eigenvalues of the operators associated with the underlying symmetries. Here, both the equations and the base solution are invariant by translation along the y axis with arbitrary amplitude, and by a translation along the x axis, possibly combined with a mirror symmetry, with an amplitude that is a multiple of the wavelength, $x \mapsto x \pm 2\pi/k$. Because of the invariance by the continuous group of translations along the y axis, the perturbation $\delta w(x, y)$ can be assumed to have a harmonic dependence [5] on the variable y; let us denote k' the associated wavenumber. Because of the invariance by the discrete set of translations and mirror-symmetries with respect to the x axis, $\delta w(x, y)$ can be searched in the form of a harmonic function of x with wavelength $2m\pi/k$, m being an integer. In the following we will restrict our analysis to $m = 0$ and $m = 1$, as higher values of m are expected to lead to a weaker coupling with the base solution $A\cos(kx)$ and so to be less favorable energetically. The unstable modes that we need to consider are therefore of the form $\cos(kx + k'y)$, $\cos(kx - k'y)$ and $\cos(k'y)$: the first two terms correspond to $m = \pm 1$ and the last term to $m = 0$. Combining them with arbitrary amplitudes A_i, we write:

$$\delta w(x, y) = A_1\cos(kx + k'y) + A_2\cos(kx - k'y) + A_3\cos(k'y), \tag{16}$$

Using trigonometric identities, the deflection of the film, including the base solution $A\cos(k\,x)$, can be then written as:

$$w(x, y) = A\,\cos(k\,x) + b\,\sin(k\,x)\,\sin(k\,q\,y) + c\,\cos(k\,x)\,\cos(k\,q\,y) + d\,\cos(k\,q\,y). \tag{17}$$

[5] Here, we recover the classical result that the different Fourier modes of the perturbation in the y direction are uncoupled at linear order in the analysis of stability.

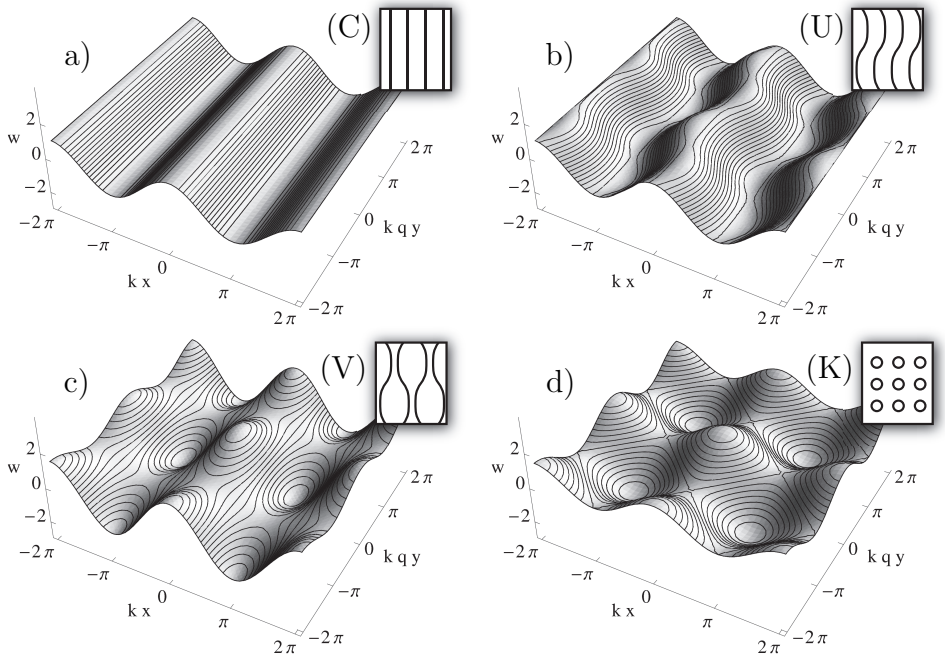

Fig. 2. Base cylindrical solution and possible unstable modes: undulating, varicose, checkerboard. The plots were obtained with the following parameters for Eq. 17: (a) $A = 1$, $b = c = d = 0$, (b) $A = 1$, $b = .5$, $c = d = 0$, (c) $A = 1$, $c = .5$, $b = d = 0$, (d) $A = d = .7$, $b = c = 0$.

where $q = k'/k$ is the rescaled longitudinal wavevector, $b = A_2 - A_1$, $c = A_1 + A_2$ and $d = A_3$. In this form, the numbers b, c and d appear as amplitudes of the undulating mode, the varicose mode and the checkerboard mode, respectively. These modes are visualized in Fig. 2. Their amplitudes b, c and d are taken to be infinitesimal in the present section which is concerned with linear stability, and small but finite in Sections 5 and 6 where the weakly post-buckled geometry is addressed.

4.2 Solving for in-plane displacement

In the present and following sections, we proceed to solve the equations of the problem in perturbations with respect to the small parameters b, c and d. We consider the deflection $w(x, y)$ to be the main unknown of the problem: our first step is to calculate the in-plane displacement (u, v) in terms of w. This involves minimizing the total energy (11) with respect to the in-plane displacement $u(x, y)$ and $v(x, y)$ only. Minimization with respect to the deflection $w(x, y)$ will be carried out in a second step, and we consider $w(x, y)$ as fixed for now. The stretching energy is the only energy contribution that depends on the in-plane displacement in equation (11). The Euler-Lagrange equations expressing the condition of stationarity of the energy with respect to $u(x, y)$ and $v(x, y)$

are the equations of in-plane equilibrium for the film:

$$\frac{\partial \sigma_{xx}}{\partial x} + \frac{\partial \sigma_{xy}}{\partial y} = 0 \quad \text{and} \quad \frac{\partial \sigma_{xy}}{\partial x} + \frac{\partial \sigma_{yy}}{\partial y} = 0. \tag{18}$$

These equations can be transformed by plugging in the definition (3) of in-plane stress $\sigma_{\alpha\beta}$ as a function of strain, and expressing the strain itself expressed in terms of the displacement by equation (2). The result is a set of two coupled *linear* partial differential equations [6] for the unknowns functions u and v, with inhomogeneous terms depending on w in a nonlinear way. We solve the resulting equations for $u(x, y)$ and $v(x, y)$. As explained above, this involves plugging in equations (3) and (2) into equation (18), and then using the trial form of the deflection in equation (17). The inhomogeneous terms in these equations are functions of the variables x and y: their Fourier decomposition is computed symbolically, and the equations for u and v are solved Fourier mode by Fourier mode (this reduces the problem to the solution of a linear system of equations, as the coupled partial differential equations are transformed into a set of linear equations for the unknown Fourier coefficients of u and v). Skipping over the details of this calculation, carried out with the help of a symbolic calculation software, one arrives at an explicit solution for the in-plane displacement:

$$\begin{aligned} u(x,y) = &-\frac{\nu\, k\, q^2}{2}\, c\, d\, \sin(kx) + \frac{k}{16}\left(2A^2 + (b^2-c^2)(\nu\, q^2 - 1)\right)\sin(2kx) \\ &+ \frac{k}{2}\, A\, b\, \sin(kqy) + \sum_{\chi=0,1}\Bigg\{ \frac{k\, q^2\,(4q^2-\nu)}{4\,(1+4q^2)^2}(b + (-1)^\chi\, c)\, d\, \sin\left(k\,(x - (-1)^\chi\, 2\, q\, y)\right) \\ &+ \frac{k}{32}(b+(-1)^\chi\, c)^2 \sin\left(2k\,(x-(-1)^\chi\, q\, y)\right) + \frac{k\, q^2\,(q^2-\nu)}{2\,(1+q^2)^2}\, A\, d\, \sin\left(k(x+(-1)^\chi\, q\, y)\right) \\ &+ \frac{k\,(8 + 2\,(2-\nu)\, q^2 + q^4)}{4\,(4+q^2)^2}\, A\,((-1)^\chi\, b + c)\, \sin\left(k\,(2x - (-1)^\chi\, q\, y)\right)\Bigg\} \end{aligned} \tag{19a}$$

[6] In the FvK plate theory, the in-plane equilibrium equations are linear with respect to u and v as the strain has been linearized with respect to these functions from the beginning.

and

$$
\begin{aligned}
v(x,y) = \frac{k\,q}{2}\,b\,d\,\sin(kx) - \frac{k\,\nu}{2q}\,A\,c\,\sin(kqy) \\
+ \frac{k}{16\,q}\left((\nu-q^2)(b^2-c^2)+2\,q^2\,d^2\right)\sin(2kqy) \\
+ \sum_{\chi=0,1}\Bigg\{\frac{k\,q\,(1+2(2-\nu)\,q^2+8\,q^4)}{4\,(1+4q^2)^2}\,(b+(-1)^\chi\,c)\,d\,\sin(k\,(x-(-1)^\chi\,2\,q\,y)) \\
-\frac{k\,q}{32}\,(b+(-1)^\chi\,c)^2\sin(2\,k\,(x-(-1)^\chi\,q\,y))+\frac{k\,q\,(\nu q^2-1)}{2\,(1+q^2)^2}\,A\,d\,\sin(k\,(x+(-1)^\chi\,q\,y)) \\
+\frac{k\,q\,(-4+\nu q^2)}{4\,(4+q^2)^2}\,A\,(b+(-1)^\chi\,c)\,\sin(k\,(2\,x-(-1)^\chi\,q\,y))\Bigg\}. \quad (19b)
\end{aligned}
$$

4.3 Energy as a function of the perturbation parameters

Having solved the Euler-Lagrange equations for $u(x,y)$ and $v(x,y)$, we have in fact determined to optimum in-plane displacement associated with a given deflection $w(x,y)$. Elimination of the in-plane displacement provides the opportunity to write the stretching energy as a function of the deflection only. Let us write $\mathcal{E}_{\text{fs}}^{\dagger}(\{w\})$ this reduced stretching energy, function of w only (as opposed to the initial energy $\mathcal{E}_{\text{fs}}$ which was a function of u and v as well):

$$
\mathcal{E}_{\text{fs}}^{\dagger}(\{w\}) = \min_{u,v} \mathcal{E}_{\text{fs}}(\{u,v,w\}). \quad (20)
$$

The reduced stretching energy $\mathcal{E}_{\text{fs}}^{\dagger}(\{w\})$ can be found by plugging the solutions (19a) and (19b) for $u(x,y)$ and $v(x,y)$ into the initial definition of stretching energy (5). Combining with the form of the deflection proposed in equation (17), carrying out the integration over the in-plane directions symbolically, and expanding the result up to quadratic terms in the small parameters

b, c and d, we find:

$$\begin{aligned}\mathcal{E}^{\dagger}_{\mathrm{fs}}(A,b,c,d,k,q) = \frac{Eh}{2\,(1-\nu^2)}\Bigg(&(\eta_x)^2 + (\eta_y)^2 + 2\nu\,\eta_x\,\eta_y - \frac{\eta_x+\nu\,\eta_y}{2}k^2A^2 \\ &+ \frac{1}{16}k^4A^4 - \frac{1}{4}(\eta_x\,(1+\nu\,q^2)+\eta_y\,(\nu+q^2))\,k^2\,(b^2+c^2) + \frac{k^2\,q^2}{2}\,(\nu\,\eta_x+\eta_y)\,d^2 \\ &+ \frac{k^4}{16\,(4+q^2)^2}\left(16+8\,(1+2\nu)q^2+(2+8\,\nu-\nu^2)\,q^4+\nu\,q^6\right)\,A^2\,b^2 \\ &+\frac{k^4}{16\,(4+q^2)^2}\left(48-32\,\nu^2+8\,(3+2\nu-2\nu^2)\,q^2+(4+8\,\nu-3\,\nu^2)q^4+\nu\,q^6\right)A^2\,c^2 \\ &- \frac{k^2\,q^2}{8\,(1+q^2)^2}(\nu+2\,(1+\nu-\nu^2)\,q^2+\nu\,q^4)\,A^2\,d^2\Bigg) \\ &+ \mathcal{O}(b^2\,c^2, c^2\,d^2, d^2\,b^2, b^4, c^4, d^4). \end{aligned} \tag{21}$$

Similarly, we can derive expressions for the bending energy of the film and for the substrate energy as functions of the amplitudes A, b, c, d and wavenumbers k and q of the film. This is much easier than for the stretching energy, as they are quadratic functions of the deflection and do not depend on u and v. They are easily computed in Fourier space, noting that there are four nonzero Fourier modes for $w(x,y)$ by equation (16): the fundamental mode with amplitude A and wavevector $(k_x,k_y)=(k,0)$, and three modes corresponding to the perturbation, with amplitudes $(c\pm b)/2$ and d, and wavenumbers $(k_x,k_y)=(k,\pm qk)$ and $(k_x,k_y)=(0,qk)$ respectively. This yields

$$\mathcal{E}_{\mathrm{fb}}(A,b,c,d,k,q) = \frac{1}{4}Dk^4\left(A^2+\frac{1}{2}(b^2+c^2)(1+q^2)^2+d^2q^4\right) \tag{22}$$

$$\mathcal{E}_{\mathrm{s}}(A,b,c,d,k,q) = \frac{1}{2}E^*_{\mathrm{s}}k\left(A^2+\frac{1}{2}(b^2+c^2)\sqrt{1+q^2}+d^2q\right) \tag{23}$$

In equations (21–23), we have derived closed form expressions for the three contributions to the energy $\mathcal{E}^{\dagger}_{\mathrm{t}}(A,b,c,d,k,q)$ of the system:

$$\mathcal{E}^{\dagger}_{\mathrm{t}}(A,b,c,d,k,q) = \mathcal{E}^{\dagger}_{\mathrm{fs}} + \mathcal{E}_{\mathrm{fb}} + \mathcal{E}_{\mathrm{s}}. \tag{24}$$

This energy is known as a function of the amplitudes A, b, c, d and wavenumbers k, q of the film, of the loading (η_x,η_y) and of material parameters. Note that this expression does not involve any approximation other than neglecting higher order terms.

In following, we rewrite this energy in dimensionless form and carry out the stability analysis of the straight stripes based on the expressions just derived.

4.4 Dimensionless quantities

We could start the linear stability analysis at this point but it is more convenient to introduce rescaled quantities first as this allows us to get rid of most of the parameters of the problem. We define the quantity

$$h^* = \frac{h}{\sqrt{12\,(1-\nu^2)}}$$

as unit of length in the transverse direction; we redefine the stiffness contrast between the two layers as

$$C = \frac{E^*\,h}{E_{\rm s}^*\,h^*}, \tag{25}$$

which is by assumption a large number (note that the previous definition of the contrast, which differs from the present one by a numeric factor $\sqrt{12(1-\nu^2)}$ of order unity, has only been used in the estimates of Section 3: it is licit to alter the definition of C by a factor of order unity). The natural unit of energy per unit area is then $E\,h/C^{4/3}$, as can be shown by balancing the various energy contributions. We rescale the various physical quantities of the problem according to:

$$\eta_x = C^{-2/3}\,\overline{\eta}_x, \quad \eta_y = C^{-2/3}\,\overline{\eta}_y, \tag{26a}$$

$$A = h^*\overline{A}, \tag{26b}$$

$$b = h^*\overline{b}, \quad c = h^*\overline{c}, \quad d = h^*\overline{d} \tag{26c}$$

$$k = C^{-1/3}\,\overline{k}/h^* \tag{26d}$$

$$\mathcal{E} = E\,h\,C^{4/3}\,\overline{\mathcal{E}}, \tag{26e}$$

where bars denote rescaled quantities, such as $\overline{\eta}_x$ or $\overline{A}$, which we now use in place of the original quantities.

4.5 Recovering the cylindrical base state

When $\overline{b} = \overline{c} = \overline{d} = 0$, most of the terms in the various contributions to the energy vanish, and one is left with a total energy $\overline{\mathcal{E}}_{\rm t}^{\dagger}(\{w\}) = \overline{\mathcal{E}}_{\rm fs}^{\dagger}(\{w\}) + \overline{\mathcal{E}}_{\rm fb}(\{w\}) + \overline{\mathcal{E}}_{\rm s}(\{w\})$ that is a biquadratic function of $\overline{A}$, i.e. a polynomial of order 4 of $\overline{A}$ containing only even powers. Minimizing with respect to $\overline{A}$ and $\overline{k}$, we obtain the harmonic profile, the rescaled wavenumber and the amplitude

of the cylindrical mode as

$$\overline{w}(\overline{x},\overline{y}) = \overline{A}\,\cos(\overline{k}\,\overline{x}) \tag{27a}$$

$$\overline{A} = 2\,\sqrt{\overline{\eta}_x + \nu\,\overline{\eta}_y - 3(1-\nu^2)} \tag{27b}$$

$$\overline{k} = 1. \tag{27c}$$

This cylindrical pattern is solution whenever the argument of the square root in the amplitude is positive:

$$\overline{\eta}_x + \nu\,\overline{\eta}_y - 3(1-\nu^2) \geq 0 \tag{27d}$$

In particular, the initial buckling threshold for isotropic compression reads (taking $\overline{\eta}_x = \overline{\eta}_y$ in the previous expression):

$$\overline{\eta}_{\rm c}^I = 3\,(1-\nu) \tag{27e}$$

We recover the results of Section 2.4 for isotropic compression, in dimensionless variables: the critical strain $\overline{\eta}_{\rm c}^I$, the wavenumber $\overline{k}$ and the amplitude $\overline{A}$ given above are the same as those in equations (12a), (12b) and (12c). As mentioned earlier, the wavenumber does not depend on the load parameters $\overline{\eta}_x$ or $\overline{\eta}_y$ and the optimal wavelength does not evolve above threshold.

4.6 Stability analysis

The cylindrical pattern is an exact solution of the FvK equations, and not merely a solution in the weakly post-buckled limit. This allows one to study the linear stability of this pattern analytically. As explained earlier, one needs to study the stability with respect to three types of patterns, the undulating stripes, the varicose and checkerboard modes, which are associated with the amplitudes $\overline{b}$, $\overline{c}$ and $\overline{d}$ respectively. The values of $\overline{A}$ and $\overline{k}$ given in equation (27) that characterize the cylindrical pattern are plugged into equations (21–24) for the energy. This yields the total dimensionless energy as a quadratic form of the variables $(\overline{b},\overline{c},\overline{d})$:

$$\overline{\mathcal{E}}_{\rm t}^{\dagger} = \beta(q,\overline{\eta}_x,\overline{\eta}_y,\nu)\overline{b}^2 + \gamma(q,\overline{\eta}_x,\overline{\eta}_y,\nu)\overline{c}^2 + \delta(q,\overline{\eta}_x,\overline{\eta}_y,\nu)\overline{d}^2. \tag{28}$$

The expressions for the functions β, γ and δ are available but they are too long to be given here.

Whenever

$$\min_q \beta(q,\overline{\eta}_x,\overline{\eta}_y,\nu) < 0, \tag{29a}$$

$$\min_q \gamma(q,\overline{\eta}_x,\overline{\eta}_y,\nu) < 0 \tag{29b}$$

or

$$\min_q \delta(q, \overline{\eta}_x, \overline{\eta}_y, \nu) < 0, \tag{29c}$$

the cylindrical buckling pattern is unstable with respect to undulations, to varicose or to checkerboard patterns, respectively. To determine when the condition (29a), for instance, is satisfied it suffices to compute the value of q for which β is minimum, to plug back the optimal value of q in this expression, and to track the changes of sign of the resulting expression for β as a function of loading parameters $\overline{\eta}_x$ and $\overline{\eta}_y$. In other words, the curve for marginal stability with respect to undulating patterns has the following implicit equation in the plane of initial differential strain $(\overline{\eta}_x, \overline{\eta}_y)$:

$$\begin{cases} \beta(q, \overline{\eta}_x, \overline{\eta}_y, \nu) = 0, \\ \frac{\partial \beta}{\partial q}(q, \overline{\eta}_x, \overline{\eta}_y, \nu) = 0. \end{cases} \tag{30}$$

Let us fix the value of Poisson's ratio, and imagine we can solve these two equations for q and $\overline{\eta}_y$ as a function of $\overline{\eta}_x$. Doing so, we obtain the *curve* of marginal stability [7] in the plane $(\overline{\eta}_x, \overline{\eta}_y)$ of loading parameters, and the wavenumber q of the linearly unstable mode. Since the explicit analytical form of the function β is available from the previous analysis, this curve of marginal stability can be plotted numerically in the plane $(\overline{\eta}_x, \overline{\eta}_y)$, for any value of ν.

The same reasoning holds for varicose and checkerboard patterns, using the functions γ or δ in place β. This yields a stability diagram with three curves denoting marginal stability, with respect to each of the potentially unstable modes.

4.7 Results

These curves of linear stability are shown in Figures 3 and 4. The first figure is for the case $\nu = .3$. The coordinates are the differential strain, namely the transverse strain $\overline{\eta}_x$ and the longitudinal strain $\overline{\eta}_y$ with respect to the direction of the straight stripes — in equation (27a), we have implicitly defined the y direction to be along the stripes.

The values of the longitudinal wavenumber $q = k'/k$ rescaled by the wavenumber k of the primary instability are indicated along the curves for marginal stability. In the case of undulating patterns, the minimum of the function β is always reached for $q = 0$; moreover, the curve of marginal stability has a very simple implicit equation, which reads $\overline{\eta}_y = \overline{\eta}_c^I$. This means that the

[7] A geometric interpretation of equations (30) is that they define (in an implicit manner) the envelope of the family of curves $\beta_q(\overline{\eta}_x, \overline{\eta}_y) = 0$ in the plane $(\overline{\eta}_x, \overline{\eta}_y)$, where q is the parameter of the family of curves $\beta_q = 0$.

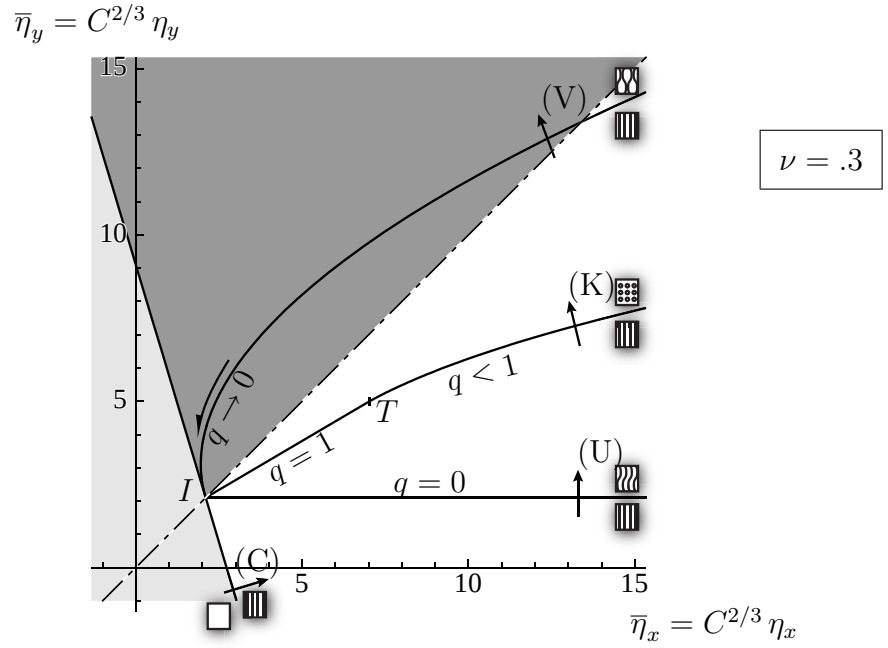

Fig. 3. Diagram of linear stability for the cylindrical pattern (straight stripes) in the plane of load parameters $(\overline{\eta}_x, \overline{\eta}_y)$, for $\nu = .3$. The dot-dashed line corresponds to the case of isotropic compression, $\overline{\eta}_x = \overline{\eta}_y$. The light grey domain in the lower left corner is where the planar configuration is stable. Its boundary is given by equation (27d). It passes through the point $I = (\overline{\eta}_{\rm c}^I, \overline{\eta}_{\rm c}^I)$ corresponding to the initial buckling threshold under isotropic loading. The dark grey region is where the cylindrical pattern exist but are unstable: when $\overline{\eta}_y > \overline{\eta}_x$, the preferred stripe orientation is along x and not y as assumed here. The three curves correspond to a loss of linear instability, from cylindrical (stripe) patterns, to either undulating (U) patterns $(\overline{b} \neq 0)$, checkerboard (K) patterns $(\overline{d} \neq 0)$, or varicose (V) patterns $(\overline{c} \neq 0)$.

cylindrical pattern becomes unstable by a long wavelength instability leading to undulating patterns, as soon as $\overline{\eta}_y \geq \overline{\eta}_{\rm c}^I$.

As indicated along the curves, the varicose instability takes place with a finite longitudinal wavelength, but this wavelength goes to infinity $(q \to 0)$ when the point I of initial isotropic buckling is approached. For checkerboard patterns, the most unstable longitudinal wavenumber is $q = 1$ along a finite portion of the curve, up to a point T beyond which q becomes strictly less than 1.

One of the striking features of this graph is that *secondary instabilities can take place right at the initial buckling threshold* as the curves of marginal stability all converge to the point I with coordinates $(\overline{\eta_x}, \overline{\eta}_y) = (\overline{\eta}_{\rm c}^I, \overline{\eta}_{\rm c}^I)$ (this is the classical threshold for the initial bifurcation into a cylindrical pattern under isotropic compression). Therefore, the cylindrical patterns cannot be observed under equi-biaxial loading, $\overline{\eta}_y = \overline{\eta}_{\rm c}^I$, as they become unstable as soon as they emerge. This surprising feature of the bifurcation diagram can be understood by recalling that there are many possible cylindrical buckling patterns above

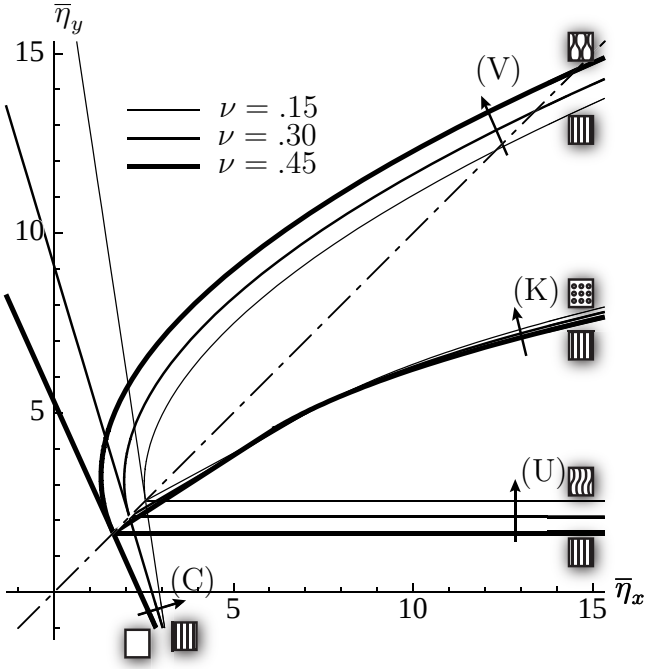

Fig. 4. Diagram of linear stability of the cylindrical patterns, for various values of Poisson's ratio of the film. We use the same conventions as in Fig. 3.

the initial threshold, corresponding to the free orientation of the generatrices in the plane of the film — imposing the generatrices to be along y was only a matter of convention. What appears as an immediate secondary bifurcation here is essentially a recombination of the many cylindrical modes available at the initial threshold, with different orientations. The checkerboard pattern, for instance, has $q = 1$ near the point I, which means that it is a superposition of two cylindrical patterns having the same physical wavenumber k and perpendicular orientations. Similarly, the instability leading to undulations takes place with large longitudinal wavelengths ($q \to 0$) near the point I, which means that it reduces locally to a change in the orientation of the cylindrical pattern.

The dependence of the bifurcation diagram on Poisson's ratio of the film is given in Figure 4. Although the curves of linear stability move with ν, the overall shape of the diagram does not change substantially.

The consequences for the patterns are as follows. In the case of anisotropic [8] loading (more accurately, for $\overline{\eta}_x > \overline{\eta}_y$, since we have assumed the stripes of primary patterns to be aligned with the y axis), the primary bifurcation, at $\overline{\eta}_x = \overline{\eta}_{\rm c}^I$, leads to cylindrical patterns that appear as stripes along the y axis.

[8] Since we use 'isotropic' as a synonym for 'equi-biaxial', we also use 'anisotropic' to denote a loading that is biaxial but not equi-biaxial.

When $\overline{\eta}_y$ reaches $\overline{\eta}_{\rm c}^I = 3(1-\nu)$ that is, in physical units

$$\eta_y \geq \eta_{\rm c}^I = \frac{1}{1+\nu}\left(\frac{3\,E_{\rm s}^*}{2\,E^*}\right)^{2/3},$$

the cylindrical patterns become unstable with respect to undulations with a large wavelength $\lambda_y \gg \lambda$ ($q=0$). In the case of a system with a finite size L, this secondary instability takes place with the smallest possible value of $q \sim 1/L$, at a threshold slightly higher than $\overline{\eta}_y = \overline{\eta}_{\rm c}^I$.

In the case of isotropic compression $\overline{\eta} = \overline{\eta}_x = \overline{\eta}_y$, the primary instability is about to take place when $\overline{\eta}$ reaches $\overline{\eta}_{\rm c}^I = 3(1-\nu)$, i.e. in physical units

$$\eta \geq \eta_{\rm c}^I = \frac{1}{1+\nu}\left(\frac{3\,E_{\rm s}^*}{2\,E^*}\right)^{2/3}.$$

Concomitantly, both the undulating stripes and checkerboard become unstable. The undulations of the stripes have again a large wavelength ($q=0$); for the checkerboard pattern, the maxima and minima of deflection are located at the vertices of a a square grid ($q=1$). The mesh size of this square grid is $\overline{\lambda} = 2\pi/\overline{k} = 2\pi$ in rescaled variables ($\overline{k}=1$), that is

$$\lambda_x = \lambda_y = \lambda = 2\pi/k = 2\pi\,h\,(E^*/(12\,E_{\rm s}^*))^{1/3}$$

in physical units.

This competition between cylindrical and checkerboard patterns has been studied before by Chen and Hutchinson (2004). However, they have set arbitrarily the mesh size of the square grid to $(\sqrt{2}\,\lambda)$, which is not the optimal checkerboard mode. As a result, they overestimate the energy of the checkerboard mode and we believe that their conclusions regarding the pattern selection are erroneous.

Under both anisotropic or isotropic load, we do not expect the varicose mode to be observed as the instability threshold from cylindrical to varicose patterns takes place at loads much larger than for undulating stripes or for the checkerboard mode. For this reason, we will not carry out the post-buckling analysis of this mode.

To summarize, two cases must be discussed. For anisotropic loading, we expect an undulating mode with large wavelength by a secondary instability affecting straight stripes; the analysis of post-buckled undulating stripes is presented in Section 5. Under isotropic loading, the undulating mode is in competition with a checkerboard mode obtained by a superposition of two cylindrical modes with identical wavelengths oriented in perpendicular directions. A nonlinear analysis is needed to study the competition between the undulating mode and the checkerboard mode in this case, see Section 6.

5 Post-buckling analysis of undulating stripes

According to the results of Section 4, the cylindrical pattern (straight stripes) first becomes unstable towards undulating stripes when loading is anisotropic (biaxial but not equi-biaxial) — see Fig. 3 in particular. This undulating pattern appears with an infinite longitudinal wavelength at secondary threshold $\overline{\eta} = 3(1-\nu)$. Under isotropic (equi-biaxial) loading, undulating stripes are important too: this is one of the few modes that can potentially be observed above threshold. In this section, undulating stripes are analyzed in the post-buckling regime.

5.1 Formulation

The procedure allowing one to compute the elastic energy of the post-buckled undulating pattern is almost the same as that for the linear stability of section 4.1. The only difference is that quartic terms in $\overline{b}$ must be retained in the stretching energy:

$$\begin{aligned}\mathcal{E}^{\dagger}_{\rm fs}(\overline{b},q) = \frac{Eh}{2C^{4/3}}\Bigg(&- \frac{1}{1-\nu^2}\left(\overline{\eta}_x + \nu\overline{\eta}_y - 3(1-\nu^2)\right)^2 \\ &- \frac{1}{4(4+q^2)^2}\Big(32 - 32\sqrt{1+q^2} + 16(\overline{\eta}_y - 1 + 3\nu)q^2 - 16q^2\sqrt{1+q^2} \\ &- \left(\overline{\eta}_x - (8-\nu)\overline{\eta}_y + 3(9-8\nu+\nu^2)\right)q^4 - 2q^4\sqrt{1+q^2} + (\overline{\eta}_y - 10 + 3\nu)q^6 - q^8\Big)\overline{b}^2 \\ &+ \frac{1}{128(1-\nu^2)}\Big(3-\nu^2+4\nu q^2+(3-\nu^2)q^4\Big)\overline{b}^4\Bigg) \end{aligned} \quad (31)$$

The substrate energy and the bending energy of the film are quadratic with respect to the variable $\overline{b}$ by definition. Their expression is not modified; they are obtained by setting $c = d = 0$ in Eqs. (22–23).

5.2 Above threshold

At a small distance above threshold, the undulating mode keeps its analytical form $\delta\overline{w} = \overline{b}\,\sin(\overline{k}\,\overline{x})\,\sin(\overline{k}\,q\,\overline{y})$, as established in weakly nonlinear perturbation theory (Manneville, 1990). We set

$$\overline{\eta}_y = 3(1-\nu) + \epsilon,$$

and take ϵ as a small parameter. The total energy $\mathcal{E}^{\dagger}_{\rm t}(\overline{b},q)$ is again minimized with respect to its parameters. This yields the wavenumber and amplitude of

the undulating mode, at lower order in ϵ:

$$q = 2\left(\frac{2}{\overline{\eta}_x + 9 + 3\,\nu}\right)^{1/2} \epsilon^{1/2}, \tag{32a}$$

$$\overline{b} = 8\left(\frac{1-\nu^2}{(3-\nu^2)\,(\overline{\eta}_x + 9 + 3\,\nu)}\right)^{1/2} \epsilon, \tag{32b}$$

and the post-buckling energy (using straight stripes as a reference):

$$\mathcal{E}_{\rm t}^{\dagger}(\overline{b}, q) - \mathcal{E}_{\rm t}^{\dagger}(\overline{b}=0) = -\frac{16\,E\,h\,(1-\nu^2)}{(3-\nu^2)\,(\overline{\eta}_x + 9 + 3\,\nu)\,C^{4/3}}\,\epsilon^4. \tag{32c}$$

The wavelength of the pattern, proportional to $2\pi/q$, is infinite at threshold and decreases as $1/(\overline{\eta}_y - 3(1-\nu))^{1/2} = 1/\epsilon^{1/2}$ above threshold. The amplitude of the perturbation on top of straight wrinkles increases linearly with the distance to threshold ϵ (note that the amplitude A of the cylindrical mode can be considered as constant above secondary threshold in a first approximation). The energy is less than that of straight stripes by an amount of order ϵ^4.

5.3 Far above threshold

Far above secondary threshold, the perturbation probably does not remain of the form $\delta\overline{w} = \overline{b}\,\sin(\overline{k}\,\overline{x})\,\sin(\overline{k}\,q\,\overline{y})$. It could be found by a systematic expansion in powers of ϵ of a solution to the whole set of equations for the film on an elastic foundation, but this is an unpleasant calculation. Here, we continue to use the same simple trial form of the deflection far above threshold; our aim is to derive approximate results concerning the behavior of undulating stripes. These results will be used in the second companion paper as a validation for an approximate buckling model introduced there (Audoly and Boudaoud, 2007b).

The total energy is minimized with respect to $\overline{b}$ and q; recall that q was defined as the ratio of the longitudinal to transverse wavenumbers k_y/k_x, which is also the ratio of the transverse to longitudinal wavelengths λ_x/λ_y where λ_x is assumed constant and given by the analysis of straight stripes. The values of the optimal rescaled longitudinal wavenumbers q are shown in Fig. 5, together with the band of wavenumbers for which there is a decrease in energy with respect to straight stripes, *i. e.* $\mathcal{E}_{\rm t}^{\dagger}(\overline{b}, q) < \mathcal{E}_{\rm t}^{\dagger}(\overline{b}=0)$; the amplitude $\overline{b}$ of the pattern with lowest energy is also given. The main results are that the (longitudinal) wavelength of undulations becomes of the same order of magnitude as the (transverse) wavelength of the cylindrical base pattern, and that the amplitude of the undulations becomes comparable to the amplitude of the cylindrical pattern.

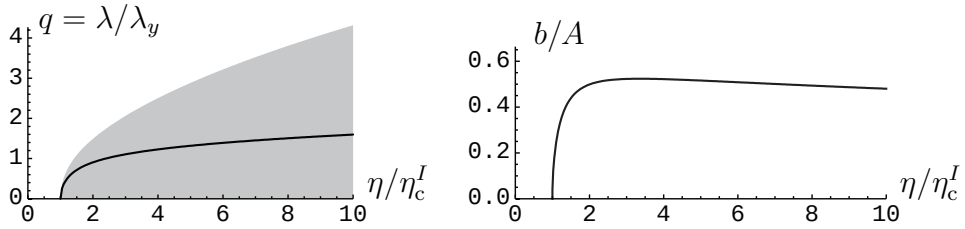

Fig. 5. Analysis of post-buckled undulating stripes under equi-biaxial compression, as a function of the compressive strain η. *Left*: range of unstable rescaled longitudinal wavenumber q (grey sector) and optimal wavenumber is plotted (curve). *Right*: amplitude b of the undulations rescaled by the amplitude of the cylindrical pattern A.

6 Post-buckling analysis of checkerboard and hexagons

In the case of isotropic loading, the linear stability analysis of the cylindrical pattern in Section 4 revealed the possibility of an instability leading to a checkerboard mode instability. Indeed, by a general result of linear stability theory (see Manneville, 1990), an isotropic system undergoing a linear instability has a whole family of linearly unstable modes available at threshold, corresponding to the free orientation of the wavevector; in this case, square or hexagon patterns are obtained generically by nonlinear coupling between these linear modes.

In this section, we analyze post-buckled checkerboard and hexagonal patterns. We focus on the case of isotropic (equi-biaxial) loading: the case of anisotropic loading does not need to be considered as checkerboards or hexagons are then superseded by undulating stripes, see Section 4. Checkerboard patterns have already been encountered in the stability analysis of section 4. Hexagonal patterns have not been discussed so far: they arise from the analysis of linear stability with $m = 2$. In Section 4.1, we have only studied the cases $m = 0$ and $m = 1$, arguing that modes with a larger values of m have a higher energy. This claim is confirmed at the end of the present section, as the hexagon patterns turn out to be less favorable than checkerboards.

6.1 Formulation

Both the checkerboard and hexagon patterns are obtained as a superposition of $n = 2$ or $n = 3$ cylindrical modes, respectively, along evenly distributed orientations, making an angle π/n with respect to each other: we consider a profile given by the superposition

$$w(x,y) = \sum_{i=0}^{n-1} A \cos\left\{k\left(x\cos\frac{\pi\, i}{n} + y\sin\frac{\pi\, i}{n}\right)\right\}, \tag{33}$$

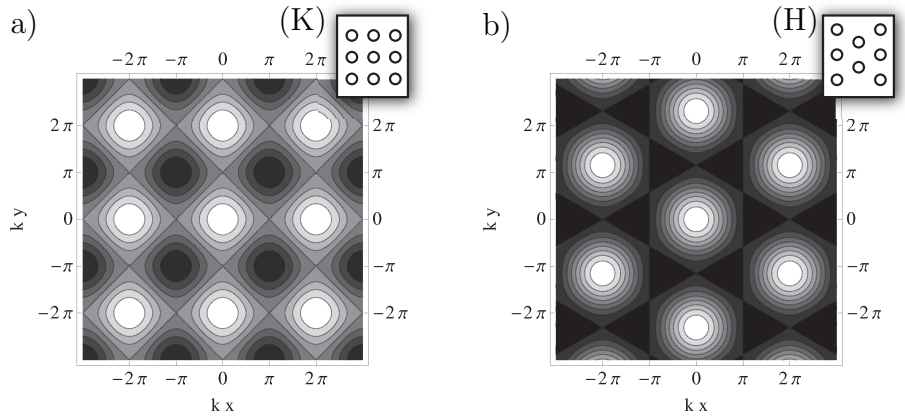

Fig. 6. Patterns obtained by superposition of n cylindrical modes with same wavelength but different orientations, see equation (33): (a) checkerboard patterns, $n = 2$; (b) hexagons, $n = 3$.

with $n = 2$ for checkerboard and $n = 3$ for hexagonal modes. For the sake of simplicity, we restrict the presentation to isotropic loading, $\eta_x = \eta_y = \eta$, and to the case where the amplitude A is the same for all the Fourier modes, indexed by i, in the superposition. In principle, theses amplitudes A_i could depend on the index i. We did investigate the general case where the amplitudes A_i can be tuned independently, and found that the case of identical amplitudes $A_i = A$ for all modes is always optimal under isotropic loading.

The bending energy of the film and the substrate energy are computed by plugging equation (33) into equations (6) and (9):

$$\mathcal{E}_{\mathrm{s}}(A, k, n) = \frac{n}{2}\, E_{\mathrm{s}}^{*}\, k\, A^2, \tag{34a}$$

$$\mathcal{E}_{\mathrm{fb}}(A, k, n) = \frac{n}{4}\, D\, k^4\, A^2. \tag{34b}$$

The stretching energy is computed along the same lines as earlier in section 4.1. We first solve equations (18) for the in-plane displacements. For checkerboards ($n = 2$), we find

$$u(x, y) = \frac{1}{4}\, A^2\, k\, \left((1-\nu)\cos(k\,x) + \cos(k\,y)\right)\, \sin(k\,x), \tag{35a}$$

$$v(x, y) = \frac{1}{4}\, A^2\, k\, \left(\cos(k\,x) + (1-\nu)\cos(k\,y)\right)\, \sin(k\,y), \tag{35b}$$

and the stretching energy reads

$$\mathcal{E}_{\mathrm{fs}}^{\dagger}(A, k, n = 2) = \frac{E\, h}{32\,(1-\nu)}\, \left(32\,\eta^2 - 16\,\eta\, A^2\, k^2 + (3-\nu)\, A^4\, k^4\right). \tag{36}$$

Similarly, for hexagons ($n = 3$), the in-plane displacement reads

$$u(x,y) = \frac{1}{8}A^2 k\Big(2\left(2(1-\nu) + (3-\nu)\cos(kx)\right)\cos(\sqrt{3}ky/2)\sin(kx/2) + (1 - 3\nu + 2\cos(kx) + \cos(\sqrt{3}ky))\sin(kx)\Big), \tag{37a}$$

$$v(x,y) = \frac{1}{8\sqrt{3}}A^2 k\Big((-4\nu + (3-\nu)\cos(kx))\sin(\sqrt{3}ky/2)\cos(kx/2) + (3 - \nu + 3\cos(kx))\sin(\sqrt{3}ky)\Big). \tag{37b}$$

When plugged into the stretching energy of the film, this yields

$$\mathcal{E}^\dagger_{\rm fs}(A,k,n=3) = \frac{E\,h}{128\,(1-\nu)}\,\left(128\,\eta^2 - 96\,\eta\,A^2\,k^2 + 3\,(11-5\nu)\,A^4\,k^4\right). \tag{38}$$

The total energy is again the sum of the three contributions

$$\mathcal{E}^\dagger_{\rm t}(A,k,n) = \mathcal{E}_{\rm s}(A,k,n) + \mathcal{E}_{\rm fb}(A,k,n) + \mathcal{E}^\dagger_{\rm fs}(A,k,n). \tag{39}$$

6.2 Results

In the following, we will use the rescaled quantities $\overline{A}$, $\overline{k}$, etc. defined in Section 4.4. In particular, the rescaled differential strain is defined as $\overline{\eta} = C^{2/3}\,\eta$. We carry out a weakly nonlinear analysis slightly above the primary threshold where, according to the results of Section 4, the films goes directly from its unbuckled configuration to either undulating stripes, a checkerboard pattern or hexagons. Slightly above threshold, we write the loading as

$$\overline{\eta} = 3\,(1-\nu) + \epsilon,$$

where ϵ is a small parameter. By minimizing the total energy $\mathcal{E}^\dagger_{\rm t}(\overline{b},q)$ we determine the buckling parameters at lower order in ϵ. For the checkerboard mode ($n = 2$), we find

$$\overline{k} = 1, \tag{40a}$$

$$\overline{A} = \left(\frac{2}{3-\nu}\right)\,\epsilon^{1/2}, \tag{40b}$$

and the energy release by buckling reads

$$\mathcal{E}^\dagger_{\rm t}(\overline{A}) - \mathcal{E}^\dagger_{\rm t}(\overline{A}=0) = -\frac{2Eh}{(1-\nu)(3-\nu)C^{4/3}}\,\epsilon^2. \tag{41}$$

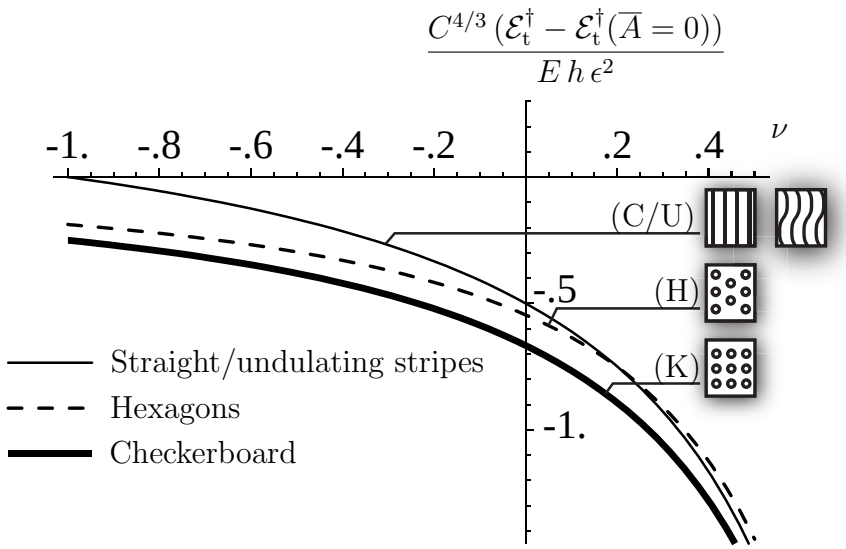

Fig. 7. Comparison of the energies of various buckling patterns for isotropic loading as a function of the Poisson ratio ν, obtained by weakly nonlinear analysis: cylinders ($n = 1$) from equation (44), checkerboard ($n = 2$) from equation (41), and hexagons ($n = 3$) from equation (43). The zero of energy is the unbuckled configuration, $\overline{A} = 0$. The three patterns in competition have the same buckling threshold; just above threshold, the energy of the checkerboard is always the lowest, for all values of Poisson's ratio. From equation (32c), the energy difference between straight and undulating stripes is of order ϵ^4 although the energy differences between all the other patterns are of order ϵ^2: straight stripes and undulating stripes with a large longitudinal wavelength are undistinguishable just above threshold.

For the hexagonal mode ($n = 3$), we find

$$\overline{k} = 1, \tag{42a}$$

$$\overline{A} = \frac{4}{\sqrt{11 - 5\nu}}\,\epsilon^{1/2}, \tag{42b}$$

and the energy release by buckling reads

$$\mathcal{E}_t^\dagger(\overline{A}) - \mathcal{E}_t^\dagger(\overline{A}=0) = -\frac{6Eh}{(1-\nu)(11-5\nu)C^{4/3}}\,\epsilon^2. \tag{43}$$

The wavelength of the two patterns remains identical to that of the cylindrical pattern. Their amplitude increases as the square-root of the distance ϵ to threshold.

The energy release of the checkerboard, the hexagons and the cylindrical pattern are compared as a function of ν in Fig.7. The energy of the cylindrical pattern is given by

$$\mathcal{E}_t^\dagger(\overline{A}) - \mathcal{E}_t^\dagger(\overline{A}=0) = -\frac{Eh(1+\nu)}{2(1-\nu)C^{4/3}}\,\epsilon^2. \tag{44}$$

In this plot, we take the unbuckled configuration ($\overline{A} = 0$) as the zero of the energy.

It appears that the checkerboard is always the most favorable. Compared to other patterns, it lowers the energy by an amount that is quadratic in the distance to threshold ϵ. Under isotropic load, we therefore expect a transition directly from the unbuckled configuration to a checkerboard pattern.

7 Conclusion

We have investigated the buckling of a thin film bound to a compliant substrate in the presence of biaxial residual compressive stress in the film. A sinusoidal cylindrical pattern with a constant wavelength λ is an exact solution of the equations of equilibrium above an initial buckling threshold (Chen and Hutchinson, 2004). This pattern appears as straight wrinkles in experiments (e.g Bowden et al., 1998). We analyzed its linear stability with respect to four possible modes:

- undulating stripes (similar to chevron or herringbone mode observed in experiments) which are obtained from straight wrinkles by lateral undulations of the crests and valleys,
- varicose which correspond to a modulation of the amplitude of the straight wrinkles, along its crests and valleys,
- checkerboard which are obtained by superposition of two perpendicular sets of straight stripes,
- hexagons which are obtained by superposition of three sets of straight stripes, at $2\pi/3$ angles.

We found that the cylindrical pattern (straight stripes) becomes unstable when compression is increased over a well-defined threshold. The pattern selected above this threshold depends on the isotropy of the residual stress in the film, as summarized in Fig. 8.

When residual compression in the film is equi-biaxial, the straight wrinkles are never a stable equilibrium solution. The mode with lowest energy above the initial buckling threshold is a checkerboard pattern with a spatial wavelength given by the wavelength λ of the classical cylindrical solution. This corrects the conclusions of Chen and Hutchinson (2004) who assign a non-optimal wavelength, $\sqrt{2}\,\lambda$, to the checkerboard pattern in their simulations and find that their energy is higher than that of herringbones. Our analysis explains the observation of checkerboard patterns in numerical simulations under equi-biaxial loading by Huang et al. (2004). Checkerboard patterns have not been reported to appear spontaneously in experiments. This might be due to the

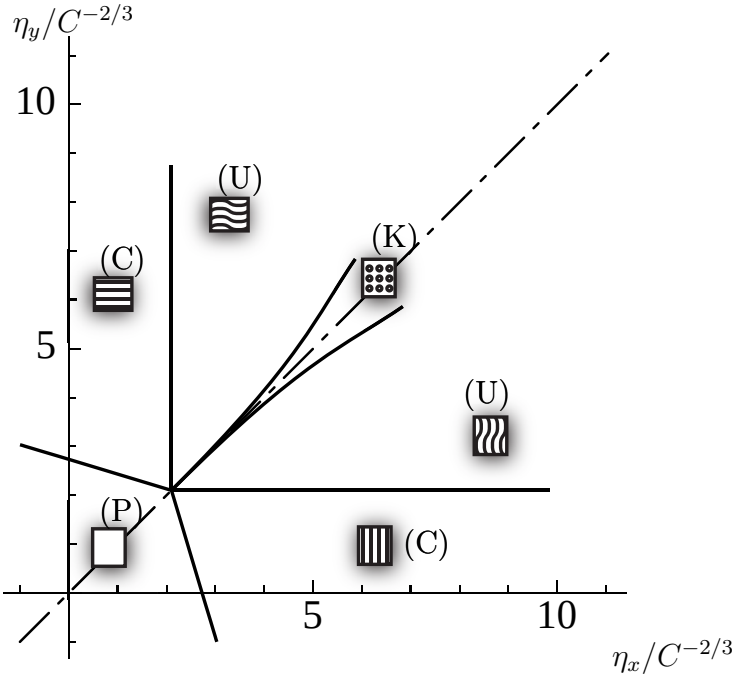

Fig. 8. Schematic phase diagram of a compressed thin film bonded to a compliant substrate: (P) unbuckled film, (C) cylindrical pattern comprising straight stripes, (U) undulating stripes, (K) checkerboard. This diagram is obtained by folding the diagram in Fig. 3 to allow the patterns to align along either principal strain direction, and complementing it with the results of the nonlinear analyses. Note that the results of the present paper are valid close to thresholds; much beyond, other patterns such as labyrinths can appear.

fact that labyrinths are more stable far enough above threshold, or that the residual stress is never perfectly isotropic nor homogeneous in the presence of imperfections. Nevertheless, Yoo et al. (2002) report that checkerboard patterns can be forced by applying and removing a micro-patterned stamp with a square grid; in numerical experiments, Huang et al. (2004) managed to select a herringbone pattern by initializing the simulation appropriately. These two observations support the existence of a competition between undulating stripes, checkerboard and herringbone patterns, as studied in Sections 5 and 6. In any case, our main result is that the checkerboard pattern minimizes the energy of the system above the *primary* buckling threshold, when load is equibiaxial.

Under anisotropic loading — more accurately, under biaxial but not equibiaxial loading —, the film first buckles into a cylindrical pattern corresponding to straight stripes, which is stable in some window of the loading parameters (η_x, η_y). At a threshold strictly above the initial threshold, this cylindrical pattern becomes unstable, see Fig. 8: the crest and valleys of the wrinkles bend while remaining locally parallel (undulating stripes), with a longitudinal wavelength that is very large at threshold ($q = 0$) and becomes comparable to the

first wavelength λ well above threshold ($q \sim 1$). In their numerical simulations with anisotropic loading, Huang et al. (2004, 2005) indeed observe the destabilization of straight to wavy wrinkles, although they do not investigate the wavelengths systematically. Our analysis of undulating patterns is also probably relevant to explain the fact that herringbones are often observed near boundaries (Bowden et al., 1998; Huck et al., 2000), where edge effects make the strain effectively anisotropic.

Again, it should be emphasized that the system may well have several equilibrium solutions (multi-stability) and that metastable solutions, which are stable but do not correspond to a global energy minimum, may well be observed in the experiments. As a matter of fact, it has been shown by Ohzono and Shimomura (2005) that thermal annealing and loading/unloading cycles can transform a labyrinthine pattern into a checkerboard-like pattern. These labyrinthine patterns have not been studied in the present paper, as they cannot be written as a linear superposition of a finite number of cylindrical linear modes; the analysis of such disordered patterns is open for future research.

We have investigated the buckling of thin films bound to compliant substrates, and obtained a rich phase diagram. The analysis of linear stability reveals that there is a family of unstable modes at threshold, corresponding to the free orientation of the straight wrinkles. Complex pattern appear very close to, or even at the primary instability threshold; although they look quite different from the well-studied one-dimensional pattern, they can be obtained as a linear superposition of such harmonic modes. We have emphasized the crucial role of the anisotropy of the loading in the pattern selection. Herringbone patterns emerges naturally from the present analysis as the extrapolation of the undulating mode to the limit of large residual stress (strongly post-buckled regime) — we refer to the companion papers (Audoly and Boudaoud, 2007b,c) for a detailed analysis.

References

Allen, H. G., 1969. *Analysis and Design of Structural Sandwich Panels*. Pergamon Press, New York.

Audoly, B., 1999. Stability of straight delamination blisters. Physical Review Letters 83, 4124–4127.

Audoly, B., Boudaoud, A., 2007b. Buckling of a thin film bound to a compliant substrat (part II). A global scenario for the formation of herringbone pattern. Submitted to Journal of the Mechanics and Physics of Solids.

Audoly, B., Boudaoud, A., 2007c. Buckling of a thin film bound to a compliant substrate (part III). Herringbone solutions at large buckling parameter. Submitted to Journal of the Mechanics and Physics of Solids.

Audoly, B., Pomeau, Y., 2008. *Elasticity and geometry: from hair curls to the nonlinear response of shells*. Oxford University Press.

Audoly, B., Roman, B., Pocheau, A., 2002. Secondary buckling patterns of a thin plate under in-plane compression. The European Physical Journal B 27, 7–10.

Bowden, N., Brittain, S., Evans, A. G., Hutchinson, J. W., Whitesides, G. M., 1998. Spontaneous formation of ordered structures in thin films of metals supported on an elastomeric polymer. Nature 393, 146–149.

Chen, X., Hutchinson, J. W., 2004. Herringbone buckling patterns of compressed thin films on compliant substrates. Journal of Applied Mechanics 71, 597–603.

Genzer, J., Groenewold, J., 2006. Soft matter with hard skin: from skin wrinkles to templating and material characterization. Soft Matter 2, 310–323.

Huang, R., 2005. Kinetic wrinkling of an elastic film on a viscoelastic substrate. Journal of the Mechanics and Physics of Solids 53, 63–89.

Huang, Z., Hong, W., Suo, Z., 2004. Evolution of wrinkles in hard films on soft substrates. Physical Review E (Statistical, Nonlinear, and Soft Matter Physics) 70, 030601.

Huang, Z. Y., Hong, W., Suo, Z., 2005. Nonlinear analyses of wrinkles in a film bonded to a compliant substrate. Journal of the Mechanics and Physics of Solids 53, 2101–2118.

Huck, W., Bowden, N., Onck, P., Pardoen, T., Hutchinson, J., Whitesides, G., 2000. Ordering of spontaneously formed buckles on planar surfaces. Langmuir 16, 3497–3501.

Jensen, H. M., 1993. Energy release rates and stability of straight-sided, thin-film delaminations. Acta Metallurgica et Materialia 41, 601–607.

Mahadevan, L., Rica, S., 2005. Self-organized origami. Science 307, 1740.

Manneville, P., 1990. *Dissipative structures and weak turbulence*. Perspectives in Physics. Academic Press, Inc., San Diego, CA.

Ohzono, T., Shimomura, M., 2005. Effect of thermal annealing and compression on the stability of microwrinkle patterns. Physical Review E (Statistical, Nonlinear, and Soft Matter Physics) 72, 025203.

Sultan, E., Boudaoud, A., 2007. The buckling of a swollen thin gel layer bound to a compliant substrate. Journal of Applied Mechanics in press.

Timoshenko, S., Gere, J. M., 1961. *Theory of elastic stability*. MacGraw Hill, New York, 2$^{\text{nd}}$ edn.

Yoo, P. J., Suh, K. Y., Park, S. Y., Lee, H. H., 2002. Physical self-assembly of microstructures by anisotropic buckling. Advanced materials 14, 1383–1387.